catalysts

MDPI

Article

# $H_2$ Thermal Desorption Spectra on Pt(111): A Density Functional Theory and Kinetic Monte Carlo Simulation Study

**Caoming Yu [1,†], Fang Wang [1,†], Yunlei Zhang [1], Leihong Zhao [1], Botao Teng [1,*], Maohong Fan [2,*] and Xiaona Liu [1]**

[1] Key Laboratory of the Ministry of Education for Advanced Catalysis Materials, Zhejiang Normal University, Jinhua 321004, China; hnyucaoming@163.com (C.Y.); wangf635@163.com (F.W.); zhangyunlei@zjnu.edu.cn (Y.Z.); zlh@zjnu.cn (L.Z.); lxn@zjnu.cn (X.L.)

[2] Department of Chemical & Petroleum Engineering, University of Wyoming, Laramie, WY 82071, USA

* Correspondence: tbt@zjnu.cn (B.T.); mfan@uwyo.edu (M.F.); Tel.: +86-139-8941-0127(B.T.)

† Caoming Yu and Fang Wang are the co-first authors.

Received: 30 August 2018; Accepted: 10 October 2018; Published: 12 October 2018


**Abstract:** Theoretical investigation of the static and kinetic behaviors of H and $H_2$ on metal surface plays a key role in the development of hydrogenation catalysts and new materials with high $H_2$ storage capacity. Based on the density functional theory (DFT) calculation of H and $H_2$ adsorption on Pt(111), H(a) adatom strongly interacts with surface Pt; while $H_2$ weakly adsorbs on Pt(111). H(a) adatoms stably occupy the face-centered cubic sites on Pt(111) which agrees with the experimental LERS observations. By using kinetic Monte Carlo (kMC) simulation, the qualitative effects of the kinetic parameters on the $H_2$ TDS spectra indicate that the $H_2$ desorption peaks shift to the low temperature with increasing pre-exponential factor and decreasing desorption barrier. Simultaneously, the desorption peaks shift downwards and broaden to two peaks with the increase of the lateral interaction energy among H(a) adatoms. Using the kMC simulation based on DFT calculation, the predicted $H_2$ TDS spectra are well consistent with the experimental ones. It unanimously proves that the two peaks of TDS spectra are derived from the lateral interactions among H(a). This work provides the intrinsic kinetics of H(a) and $H_2$ on Pt(111) at an atomic level, and gives insight into the development of hydrogenation catalysts.

**Keywords:** density functional theory; kMC simulation; Pt(111); thermal desorption spectra; hydrogen

## 1. Introduction

The adsorption and reaction behaviors of H and $H_2$ on metals are of great significance due to the wide application of hydrogenation reactions in heterogeneous catalysis [1–7]. It also provides basic information for the development of new materials with high $H_2$ storage capacity [8–11]. As a typical modeling system, the interactions between hydrogen and Pt(111) have attracted much interest and have been widely studied in experiment and theory [12–20].

Using high-resolution electron energy loss spectroscopy (HREELS), low-energy electron diffraction (LEED) and thermal desorption spectra (TDS), some consensus issues have been reached. $H_2$ dissociatively adsorbs on Pt(111) at low temperature; the maximum coverage of hydrogen ($\theta_H$) is up to one monolayer (ML) below 100 K [21]; $\theta_H$ gradually decreases with the increase of temperature [22,23]; H adsorbs at the face-centered cubic (fcc) site verified by using low-energy recoil scattering (LERS) spectra [24,25]; diffusion activation energy of H on Pt(111) is much lower than that of $H_2$ desorption. These experimental conclusions were also supported by the related theoretical works [17–21,26–28]. Gudmundsdóttir et al. [17] investigated the H adsorption behaviors

on Pt(110)-(1×2) by DFT calculations and found that the binding energy and activation energy for desorption are strongly dependent on hydrogen coverage. Thermodynamic description of hydrogen electroadsorption on Pt(111) was calculated by Hanh et al. [18] using first principles. Combining with a Monte Carlo simulation, the predicted cyclic voltammetry data is consistent with the experimental one. Hydrogen adsorption on Pt(100), (110) and (111) at high coverage was reported by Shi et al. [19] using thermodynamics based on DFT calculations. Their results indicated that hydrogen adsorption might modify the morphology of Pt catalysts. Karlberg et al. [20] proposed a cyclic voltammogram for H on Pt(111) and (100) from first principles. Combining experimental study of the H-D exchange reaction and first principles calculations, Xu [21] found that the repulsive interactions between H(a) increase with H(a) coverage, which leads to a reduction in both the adsorption energy and the desorption activation energy. Olsen et al. [26] found that a DFT/GGA approach with scalar relativistic effects is capable of describing the interaction between H(a) and Pt(111). The theoretical results by Watson et al. [27] indicated that H(a) diffusion barrier on Pt(111) is considerably smaller than that on Ni(111) and Pd(111) surfaces. By using the extended Hückel molecular orbital theory, Papoian [28] also found that H(a) moves freely on Pt(111).

Despite of the extensively studies of H/Pt(111) system, there are still some issues in debate. Christmann et al. [23] and Xu et al. [21] both reported that two $H_2$ desorption peaks at the low and high temperatures were observed in the TDS spectra on Pt(111). Since there is only one stable configuration for H adsorbed at the fcc sites on Pt(111) which has been proved by both experimental and theoretical results, what is the main reason leading to the two peaks? Which factors do determine the peak position and area of $H_2$ TDS spectra? Are the factors of $H_2$ desorption barrier ($E_a$), collision frequency among H(a) (pre-exponential factor, $v$), or the lateral interaction energy among H(a) on Pt(111) ($E_{int}$), etc.? What are the qualitative and quantitative effects for $E_a$, $v$ and $E_{int}$ on the $H_2$ TDS spectra? These important questions have still not been reported in the literature.

With the rapid development of multi-discipline cooperation in the study of the chemical reaction mechanism, kinetic Monte Carlo (kMC) simulation based on density functional theory (DFT) calculation has been applied in exploring the catalytic reaction mechanism [10,29–31]. The reaction thermodynamics and the potential energy surfaces of the possible reaction pathways on the modeling catalysts can be calculated by DFT theory [32–36]; while the kinetic reaction information on the specified surface can be obtained by the kMC simulation [30,37–41]. Hence, kMC simulation based on DFT calculation might provide the important information for the rational design of catalysts [42,43].

In this work, using DFT calculation, the adsorption, diffusion and desorption behaviors of H(a) and $H_2$ on Pt(111), as well as their electronic interactions are obtained. Then, the effects of $H_2$ desorption barrier, collision frequency and the lateral interactions among H(a) on the $H_2$ TDS spectra, are systematically investigated by kMC simulation. Finally, we combine the DFT calculation and kMC simulation to explore the intrinsic kinetics of the $H_2$ TDS spectra on Pt(111). This work provides important information regarding the interactions between H and metal materials, and sheds insight into the development of hydrogen storage material and hydrogenation catalysts.

## 2. Results and Discussion

### *2.1. DFT Study of $H_2$ and H on Pt(111)*

We systematically investigated the adsorption behaviors of H and $H_2$ on Pt(111) by density functional theory calculation. The optimized structures are shown in Figure 1 and the corresponding parameters are listed in Table 1. It can be learned from Table 1 that the adsorption energy of H(a) at the top site of surface Pt is −8.35 kcal/mol with the Pt-H bond length of 1.572 Å. The adsorption energies of H(a) at the fcc and hcp sites are −8.86 kcal/mol and −7.47 kcal/mol, respectively. The corresponding bond lengths of Pt-H are 1.866~1.879 Å. These results are well consistent with those reported by Graeme et al. [27] and Källén et al. [44].

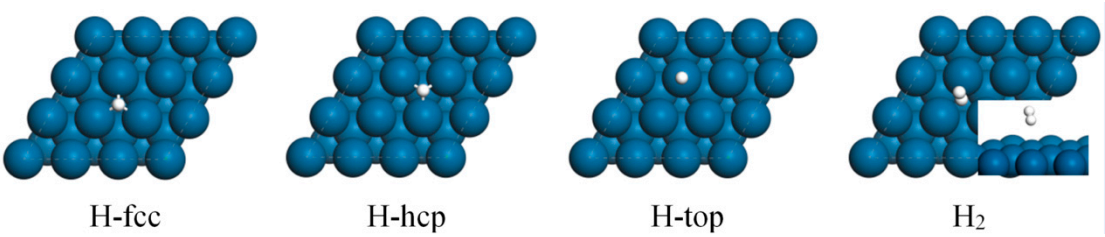


**Figure 1.** Structures of H(a) and $H_2$ on Pt(111). The dark blue and white balls represent Pt and H atoms.

**Table 1.** Parameters of H(a) and $H_2$ on Pt(111).

| | $E_{ads}$/kcal/mol | ZPVE Corrected $E_{ads}$/kcal/mol | $d_{Pt-H}$/Å | $d_{H-H}$/Å | Bader Charge/e | |
|---|---|---|---|---|---|---|
| | | | | | H | Pt |
| H-fcc | −8.86 | −9.12 | 1.874<br>1.872<br>1.875 | | −0.100 | −0.027<br>0.059<br>−0.019 |
| H-hcp | −7.47 | −7.89 | 1.879<br>1.866<br>1.878 | | −0.057 | −0.062<br>0.036<br>−0.004 |
| H-top | −8.35 | −7.35 | 1.572 | | −0.035 | 0.029 |
| $H_2$-fcc | −0.09 | 0.13 | 3.789<br>3.712<br>3.536 | 0.748 | 0.025<br>−0.032 | |

Since the adsorption energy difference between H-top and H-fcc configurations on Pt(111) is just 0.51 kal/mol, the zero-point vibrational energies (ZPVE) are further calculated to determine which one is the most stable structure. The adsorption energies at the top and fcc sites are −7.35 and −9.12 kcal/mol, respectively. Therefore, H(a) at the fcc sites is the most stable configurations for H(a) on Pt(111), which is well consistent with the experimental results [24,25]. However, the adsorption energy of $H_2$ on Pt(111) with and without the ZPVE energy is 0.13 and −0.09 kcal/mol, respectively. The H-H bond length is 0.748 Å, which is almost the same as that of free $H_2$ molecule. Meanwhile, the distances of Pt-H are larger than 3.5 Å. This indicates the very weak interaction between $H_2$ and Pt surface. This will be further proved by the following analysis of the electronic properties of H(a) and $H_2$ on Pt(111).

To explore the electronic interactions of H(a) and $H_2$ with Pt(111), charge density differences (CDD) are calculated and shown in Figure 2. It is defined as: $\Delta\rho = \rho_{adsorbate/slab} - \rho_{slab} - \rho_{adsorbate}$, where $\rho_{adsorbate/slab}$ is the charge density for the adsorbed system; $\rho_{slab}$ and $\rho_{adsorbate}$ are the charge densities for the non-interacting slab substrate and adsorbate, respectively. The yellow and grey–blue parts represent the accumulation and depletion electrons, respectively.

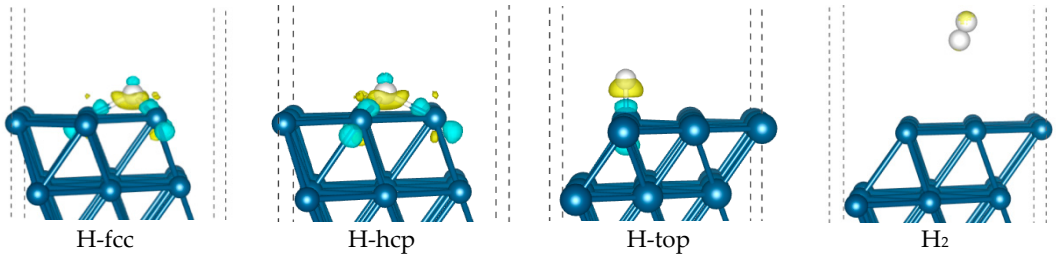


**Figure 2.** Charge density difference (CDD) of H(a) and $H_2$ on Pt(111). The isosurface value is 0.005 e/$a_0^3$.

As shown in Figure 2, H(a) atom gains electrons from the d orbital of surface Pt atoms; meanwhile the strong Pt-H bonds form due to the electron share between Pt and H(a). However, the electron transfer between $H_2$ and Pt(111) is almost negligible, which is consistent with the very weak interactions with the adsorption energy of −0.09 kcal/mol. This conclusion is also in agreement with the result of

Bader charge as listed in Table 1. That is, H(a) gains electrons with negative charge; Pt loses electrons with partially positive charge.

As shown in the partial density of states (PDOS) of H(a) in Figure 3a, the s peaks of H(a) broaden and shift to −8~−6 eV for H-fcc and H-hcp configurations and −6~−4 eV for H-top in comparison with the free radical H atom. Meanwhile, there are the corresponding electronic peaks of Pt at the same energy position, as shown in the green peaks of Figure 3b. This indicates the strong interactions between H(a) and Pt(111). However, the PDOS peak shape of $H_2$ on Pt(111) remains unchanged, and the corresponding peaks of Pt are almost the same as those of the non-interacting substrate. Therefore, the very weak interactions between $H_2$ and Pt(111) occur.

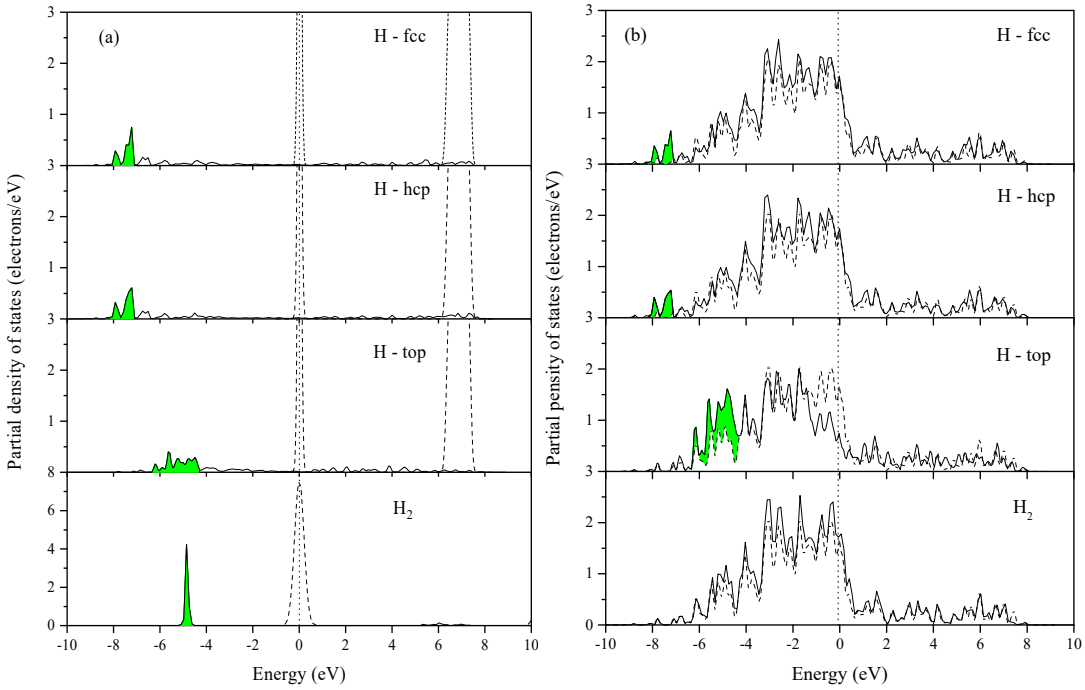


**Figure 3.** Partial density of states of adsorbates (**a**) and Pt atom near adsorbates (**b**). The vertical dot line indicates the adjusted Fermi level at 0 eV.

### *2.2. kMC Simulation of $H_2$ TDS on Pt(111)*

Before the kMC simulation of $H_2$ TDS on Pt(111) based on DFT calculation is performed, it is necessary to give a qualitative analysis of the effects of the main kinetic parameters on $H_2$ TDS on PT(111). This is very important for exploring the key parameters in kMC simulation.

A surface of 128 × 128 Pt atoms is adopted with the different H(a) coverages, in which H(a) atoms are randomly populated on Pt(111). The pre-covered H(a) models with different coverages mimic the experimental ones, in which different doses of gas atomic hydrogen are exposed to Pt(111) [21]. The samples with different H(a) coverages are heated from 100 K to 600 K with a heating rate of 10 K/s, which also agrees with the ultrahigh vacuum experimental conditions [21]. The $H_2$ TDS spectra include the following processes.

(1) H adatom diffusion: $H(*) + * \rightarrow * + H(*)$
(2) $H_2$ desorption: $2H(*) \rightarrow H_2(g) + 2*$
(3) $H_2$ dissociation: $H_2(g) + 2* \rightarrow 2H(*)$

The asterisk * with and without species denotes an adsorbed species and empty surface site, respectively. Since the Leybold stainless-steel UHV chamber is continuously vacuuming with the total pressure of about $10^{-8}$ Pa [21], the desorbed $H_2$ molecules will be quickly pumped out of the UHV chamber. Therefore, the dissociation of $H_2$ is not involved in the kMC simulation.

To explore the intrinsic kinetics of $H_2$ TDS spectra on Pt(111), we investigate the effects of the different kinetic parameters on the spectra, as shown in Figures 4–6.

### 2.2.1. Effects of the Pre-Exponential Factor of $H_2$ Desorption

As shown in Figure 4, one symmetric desorption peak is observed in the $H_2$ TDS spectra at the low (0.12 ML), medium (0.6 ML) and high (1.0 ML) coverages, respectively. The peaks shift to the low temperature with the increase of pre-exponential factor ($v$). Since the pre-exponential factor represents the collision frequency of reactants upon reaction, the higher $v$ leads to the more possibility of H(a) desorption at the same temperature. Therefore, the peak of $H_2$ TDS shifts downwards with the pre-exponential factor. Meanwhile, the peaks become higher and narrower than those of $v = 10^{12}$ $s^{-1}$.

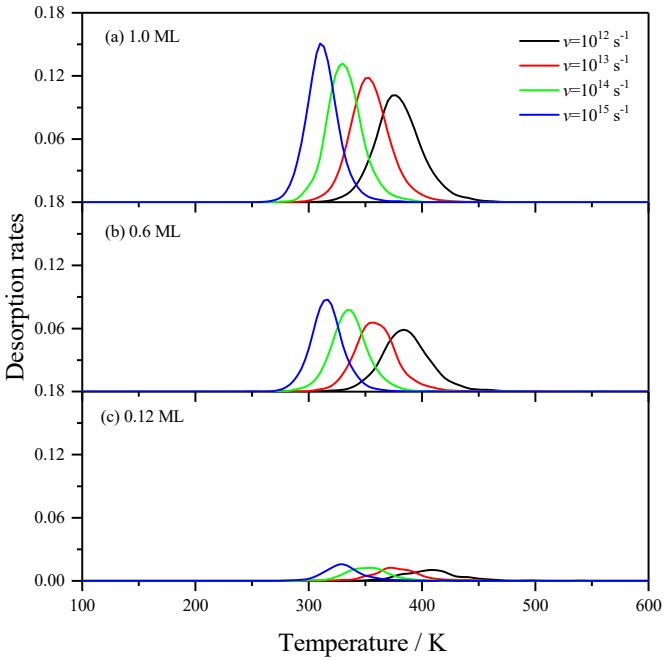


**Figure 4.** Effects of the pre-exponential factors on the $H_2$ TDS spectra. $E_a$ = 22 kcal/mol, $E_{int}$ = 0 kcal/mol.

### 2.2.2. Effects of the Desorption Barrier of $H_2$ Desorption

Similar results are observed for the $H_2$ TDS spectra on Pt(111) with the decrease of activation energy for H(a) desorption ($E_a$). That is, only one desorption peak is observed in Figure 5, and it shifts downwards with the decrease of $E_a$. Because the H(a) desorption rates increase with the low desorption barrier at the same temperature, the peak of $H_2$ TDS spectra shifts downwards with the decrease of $E_a$. Similarly, the corresponding desorption peaks also become higher and narrower than those of $E_a$ = 24 kcal/mol.

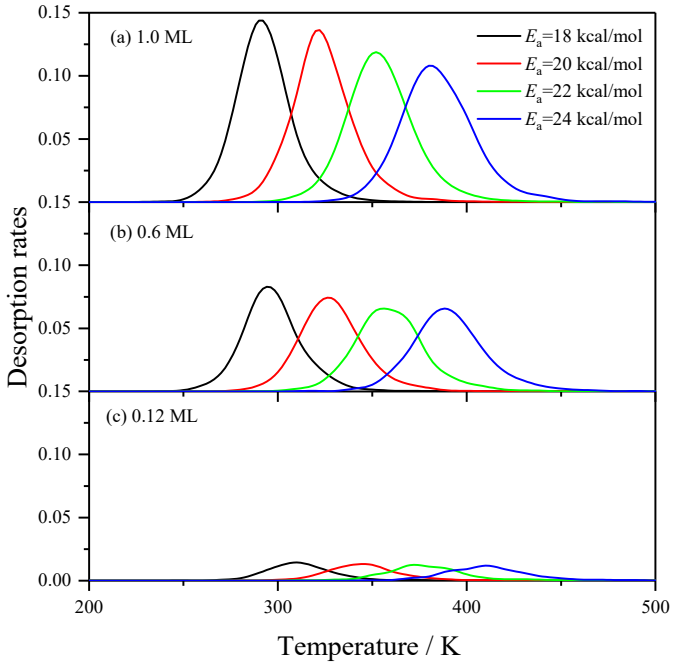


**Figure 5.** Effects of the H(a) desorption barrier on the $H_2$ TDS spectra. $v = 10^{13}$ $s^{-1}$, $E_{int}$ = 0 kcal/mol.

### 2.2.3. Effects of the Lateral Interactions among H(a)

To systematically investigate the effects of the lateral interactions among the nearest-neighbor H(a) on the $H_2$ desorption behaviors, the $H_2$ TDS spectra on Pt(111) with the different lateral interaction energies at the low, medium and high coverages are simulated and shown in Figure 6.

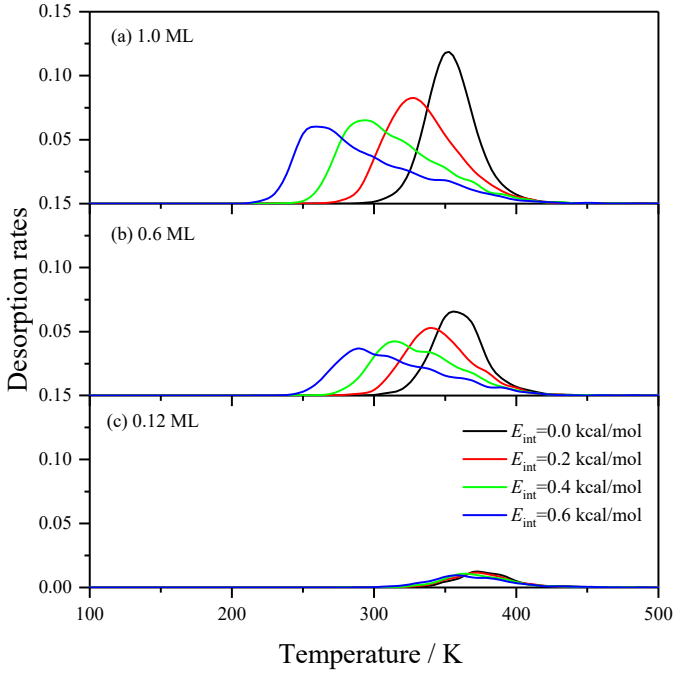


**Figure 6.** Effects of the lateral interactions among H(a) on the $H_2$ TDS spectra. $v = 10^{13}$ $s^{-1}$, $E_a$ = 22 kcal/mol.

At the low coverage (0.12 ML), the $H_2$ desorption peaks at 390 K almost remain unchanged with increasing the lateral interaction energy ($E_{int}$). This might be attributed to the large distance among

H(a) species at the low coverage, which leads to the invalid lateral interaction effects on the TDS spectra. If the H(a) coverage increases to 0.6 ML, the main desorption peaks shift to 350, 320 and 290 K corresponding to the $E_{int}$ of 0.2, 0.4 and 0.6 kcal/mol, respectively. Meanwhile, two peaks appear when $E_{int}$ is larger than 0.2 kcal/mol. When the coverage is up to 1.0 ML, the highest desorption peaks shift to 330, 290 and 260 K with $E_{int}$, respectively. This is attributed to the strong effects of the lateral interactions, which leads to the decrease of the desorption barrier of H(a) species.

### *2.3. kMC Simulation of $H_2$ TDS on Pt(111) Based on DFT Calculation*

#### 2.3.1. Parameters Calculated by DFT Method

According to the qualitative analysis of the effects of main kinetic parameters on $H_2$ TDS spectra, it indicates that the activation energies of $H_2$ desorption, pre-exponential factors and the lateral interaction energy of H(a) play the important roles in the kMC simulation of $H_2$ TDS on Pt(111). Hence, the key parameters should be calculated by the DFT method before the kMC simulation based on first principles.

The predicted barriers of $H_2$ desorption and H(a) diffusion on Pt(111) are shown in Figure 7. It can be drawn from Figure 7 that the desorption barrier of $H_2$ on Pt(111) is 21.29 kcal/mol. For the transition state structure, two H(a) atoms move to the top site of surface Pt atom with the Pt-H bond lengths of 1.691 and 1.754 Å, respectively. The distance between the two H(a) is 0.967 Å. If they are further close to each other, $H_2$ forms and desorbs from Pt(111) surface. The image frequency of TS structure is 377 $cm^{-1}$, which its vibration direction points to the dissociated H(a) and $H_2$, respectively. The diffusion barrier of H(a) at the fcc site to hcp site is 1.71 kcal/mol via a bridge site with the H-Pt bond lengths of 1.832 Å.

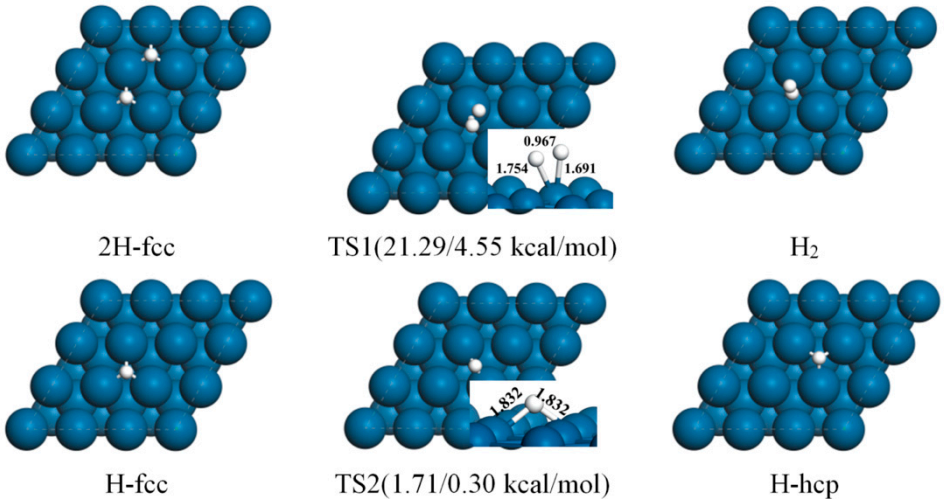


**Figure 7.** Reactants, transition states and products of $H_2$ desorption and H(a) diffusion on Pt(111).

Based on the harmonic transition-state theory, the pre-exponential factors ($\nu_i$) of each reaction step are calculated using the following equation: $v_i = \frac{\prod_1^{3N} f_i^{IS}}{\prod_1^{3N-1} f_i^{TS}}$, where $f_i^{IS}$ is the vibrational frequency at the initial state, and $f_i^{TS}$ is the vibrational frequency at the transition state (excluding the imaginary one). For the reverse pathway, the vibrational frequencies at the final state ($f_i^{FS}$) are used. Frequencies used to calculate the pre-exponential factors are listed in Tables S2–S4 of the supplementary materials.

It is reported that the lateral interactions among H(a) are mainly derived from the short-range pair interaction by the nearest neighbor (NN) adsorbates through surface, and the interactions among the next nearest neighbor (NNN) H(a) adatoms are generally negligible [21,45]. Therefore, the lateral interactions among the NN H(a) are calculated by DFT theory in this work. Since the lateral interactions among H(a) atoms are relatively weak, four models shown in Figure 8 are designed

to obtain the accurate value. The lateral interaction energy is calculated by the following equation: $E_{\text{int}} = \frac{1}{m}\left(\frac{1}{n}E_{\text{nHads}} - E_{\text{1Hads}}\right)$, where $n$ is the number of H(a); $m$ is the number of pairwise interactions per H(a) atom. The corresponding parameters are listed in Table 2.

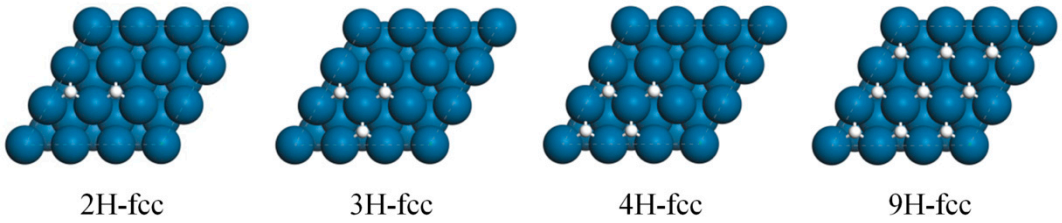


**Figure 8.** Models for calculating the lateral interaction energy of H(a) on Pt(111).

**Table 2.** Parameters of lateral interaction energy among H(a) adatoms.

| | $E_{ads}$/kcal/mol | $E_{av}$/kcal/mol | $E_{int}$/kcal/mol | $m$ |
|---|---|---|---|---|
| 1H-fcc | −8.86 | −8.86 | - | 0 |
| 2H-fcc | −16.93 | −8.46 | 0.39 | 1 |
| 3H-fcc | −24.49 | −8.16 | 0.35 | 2 |
| 4H-fcc | −31.41 | −7.86 | 0.40 | 2.5 |
| 9H-fcc | −61.55 | −6.85 | 0.34 | 6 |

Note: $m$ is the number of pairwise interactions per H(a) atom.

It can be learned from Table 2 that the average adsorption energies of H(a) decrease with coverage, which is derived from the lateral interactions among H(a). The number of pairwise interactions per H(a) atom for the $n$H-fcc ($n$ = 2, 3, 4 and 9) on Pt(111) are 1, 2, 2.5 and 6, which corresponds to the lateral interaction energies are 0.39, 0.35, 0.40, 0.35 kcal/mol, respectively. Therefore, the average value of 0.37 kcal/mol is adopted in the following kMC simulation based on DFT calculation.

#### 2.3.2. kMC Simulation Based on DFT Calculation

For the kMC simulation based on DFT calculation, all the parameters should be used by the theoretical predictions. However, the diffusion barrier of H(a) on Pt(111) is just 1.71 kcal/mol, indicating that most of computer time will be consumed in the calculation of rate constant by using the Arrhenius equation due to the very low diffusion barrier. To improve the efficiency of kMC simulation, the effects of H(a) diffusion rates are tested and shown in Figure S1 in the supplementary material. Based on the tests, the diffusion rate constant has no effects on the kMC simulation results if it is larger than 10 $s^{-1}$. In this work, the rate constant of 1000 $s^{-1}$ is adopted.

The $H_2$ TDS spectra calculated by the kMC simulation based on DFT method at different coverages are shown in Figure 9. It can be learned from Figure 9 that the desorption peak at 0.05 ML is at 345 K, which is well consistent with the experimental value of 343 K [21]. It shifts to the low temperature with the increase of H(a) coverage. When the coverage is larger than 0.6 ML, two peaks are observed. Furthermore, the desorption peak at the low temperature shifts to 250 K when the coverage is up to 1.0 ML. This is also consistent with the experimental peak temperature at 235 K in TDS spectra [21]. The $H_2$ TDS spectra derived from the kMC simulation based on DFT method unanimously prove that the two desorption peaks are derived from the lateral interactions among H(a) species. The simulation results are well consistent with those in experiment, indicating the method of kMC based on DFT calculation is feasible and reliable.

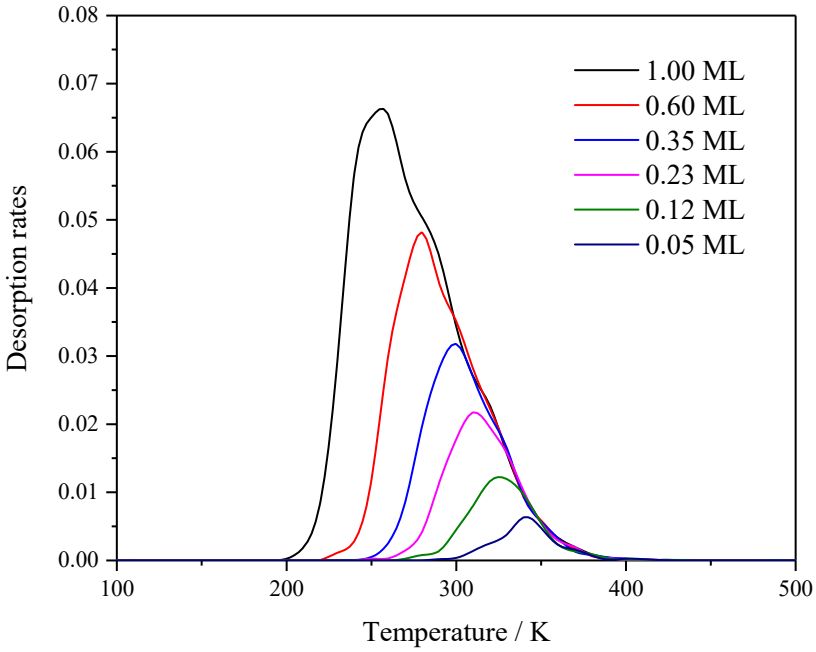


**Figure 9.** $H_2$ TDS spectra calculated by kMC simulation based on DFT calculation.

## 3. Model and Method

### *3.1. DFT Calculation Details*

Spin-polarization calculations were performed using Vienna ab initio simulation package (VASP) code based on a first-principles density functional theory [46,47]. The electron exchange and correlation were treated within the generalized gradient approximation (GGA) of the revised Perdew Burke Ernzerhof (RPBE) functional [48]. The Kohn–Sham one-electron wave functions were expanded in a planewave basis with a cutoff energy of 400 eV. The Brillouin-zone integration was approximated by a sum over special *k*-points using the Monkhorst-Pack (MP) [49] grids and Methfessel–Paxton smearing method with a sigma value of 0.1 eV. The electrons in Pt 6s, 5d and H 1s orbitals were treated as valence electrons. The ionic cores were represented by the projector augmented wave (PAW) potentials [50]. The Kohn–Sham equations were solved self-consistently. The self-consistent field tolerance for the energy calculation was set as $1.0 \times 10^{-4}$ eV; the maximum Hellmann–Feynman force tolerance for the structure optimization was set as 0.02 eV/Å.

The calculated bulk lattice constant (3.997 Å) of Pt(111) with a MP grid of $13 \times 13 \times 13$ agrees well with the experimental value (3.924 Å) and the values reported in the literature [27,28]. A Pt(111) slab model with five layers was chosen for the theoretical calculations. The two bottom layers were fixed during geometric optimization. The vacuum space was set as 12 Å along the (111) direction to minimize the interaction between slab surfaces. The p(3×3) (R = 60°) lateral cell was involved in the present work with the *k*-points grid of $3 \times 3 \times 1$. By testing the convergence of *k*-points, cutoff energy and size of Pt(111) slab, these settings ensure the required precision.

The total adsorption energy of *n*H(a) on Pt(111) was defined as $E_{ads}$=$E_{nH/slab} - (E_{slab} + 0.5nE_{H2})$, in which $E_{(nH/slab)}$, $E_{(slab)}$, and $E_{(H2)}$ represent the total energies of a slab model with adsorbed hydrogen atoms, the slab, and free hydrogen molecule, respectively. The average adsorption energy per H(a) on Pt(111) was calculated by $E_{av} = E_{ads}/n$. The adsorption energy of $H_2$ was defined as $E_{ads} = E_{H2/slab} - (E_{slab} + E_{H2})$. The vibrational properties were calculated on the basis of the harmonic vibration of the adsorbed H(a) and $H_2$(a) on Pt(111). The zero-point vibrational energy (ZPVE) is calculated by the equation of $E_{ZPVE} = \frac{1}{2}\sum_{i=1}^{n} f_i$, where $f_i$ is the energy of *i*th vibrational mode, and its unit should be converted from $cm^{-1}$ to kcal/mol or eV. The frequencies used in ZPVE corrections

were listed in Table S1. Transition states (TS) of H(a) desorption and diffusion were calculated with the climbing image nudged elastic band (CINEB) method [51]. The activation barrier was defined as the total energy difference between the transition state and the corresponding stable structures of reactants or products.

Since it was reported that the van der Waals interactions between adsorbates and surfaces do influence the adsorption and reaction behaviors of reactants and intermediates [52,53], we also compared the adsorption energies of H(a) and $H_2$ on Pt(111), as well as the barriers of H(a) diffusion and $H_2$ desorption using DFT and DFT-D methods with RPBE and PBE functionals, as listed in Table S5. The theoretical results by the two methods with PBE functional are almost the same. This might be due to two facts. One is that the volume of hydrogen atom is very small, which leads to the negligible interactions between nH-fcc through space. The other is that the lateral interactions of nH-fcc are mainly derived from the repulsive ring among H(a) through Pt(111) surface, which the corresponding electronic repulsive interactions can be well calculated by DFT method. Therefore, the results calculated by DFT method are reliable.

### *3.2. kMC Simulation*

The kMC simulation was carried out on a periodic p(128×128) (R = 60°) superlattice of Pt(111) surface, which represents the single crystal surface of Pt(111) in the ultrahigh vacuum chamber. According to the experimental results, H atoms only adsorb at the face-centered cubic (fcc) site of Pt(111); while $H_2$ very weakly physisorbs on Pt(111). Hence, the initial model of H(a) on Pt(111) with a designated coverage was produced by H random distribution at the fcc sites on Pt(111). The temperature-programmed desorption rate of H at Pt(111) was set as 10 K/s. The rate constants of the elementary surface step follow the Arrhenius equation: $r_D = v\exp(-E_a/kT)$, where $v$ is the pre-exponential factor; $T$ is the temperature, and $E_a$ is the activation barrier for the elementary processes [40,54]. The quantitative effects of the lateral interactions on the $H_2$ desorption barrier is described by the effective activation energy defined as: $E_{eff} = E_a - \sum xE_{int}$, where $E_a$ is the activation energy of H(a) desorption at zero coverage; $x$ is the number of nearest-neighbor H(a); $E_{int}$ is the lateral interaction energy [31]. According to the definition, the effects of the lateral interactions on the transition state originate from an interpolation between the initial and final states due to the repulsion among the nearest neighbor H(a). The probability of a process to be chosen and implemented is directly proportional to the rate calculated by the master equation: [40] $\frac{dP_\alpha}{dt} = \sum_\beta (k_{\alpha\beta}P_\beta - k_{\beta\alpha}P_\alpha)$, in which α and β are the adsorbates at the different sites; $P_\alpha$ and $P_\beta$ are their probabilities of forming α and β; $k_{\alpha\beta}$ is the rate constant of α transforming into β. The master equation was solved by the discrete event simulation algorithm. There are many kMC simulation programs, such as CARLOS [55], Multi-scale KMC [56] and kmos [57], etc. The program herein was written in C language [58]. The first reaction method with the time-dependent rate constants was adopted in the work. A tentative time was calculated for every possible process [42]. Consequently, the numbers of steps of the temperature programmed desorption simulation could be obtained.

## 4. Conclusions

According to the DFT calculation of H and $H_2$ adsorption on Pt(111), H(a) at the fcc site is the most stable structure. Strong interactions between H(a) and surface Pt occur; while $H_2$ weakly physisorbs on Pt(111). According to the qualitative effects of the kinetic parameters on the $H_2$ TDS spectra, it is found that the desorption peaks shift to the low temperature with increasing $v$ and decreasing $E_a$ of $H_2$ desorption. Simultaneously, the desorption peaks become higher and narrower. With the increase of $E_{int}$, the desorption peaks shift downwards and broaden to two peaks. By the kMC simulation based on DFT method, the predicted $H_2$ TDS spectra are well consistent with the experimental ones. This work provides the intrinsic kinetics of H(a) and $H_2$ on Pt(111) at the atomic level, and gives insight into the development of hydrogen storage material and hydrogenation catalysts.

**Supplementary Materials:** The following are available online at http://www.mdpi.com/2073-4344/8/10/450/s1. Table S1: Frequencies of H(a) on Pt(111) and $H_2$. Table S2: Frequencies of 2H-fcc, transition state and $H_2$. Table S3: Frequencies of H-fcc, transition state and H-hcp. Table S4: The pre-exponential factors of $H_2$ desorption and H(a) diffusion. Table S5: $E_{ads}$(eV) of the typical configurations of H(a) and $H_2$; $E_a$ of H(a) diffusion and $H_2$ desorption on Pt(111) by DFT and DFT-D methods. Figure S1: Effects of the diffusion rate constant on the $H_2$ TDS spectra by kMC simulation.

**Author Contributions:** Conceptualization, B.T.; Methodology and Software, C.Y. and F.W.; Formal Analysis, Y.Z., L.Z. and X.L.; Data Curation, C.Y. and F.W.; Writing: Original Draft Preparation, C.Y.; Writing: Review and Editing, B.T. and M.F.

**Funding:** This research was funded by the National Natural Science Foundation of China, grant number 21872125 and 21373187 and the Chinese National Undergraduate Innovation and entrepreneurship training program, grant number 201610345013.

**Acknowledgments:** This work was supported by the Synfuels China Co. Ltd. and the School of Energy Resources at University of Wyoming.

**Conflicts of Interest:** The authors declare no conflict of interest.

## References

1. Baxter, E.T.; Ha, M.A.; Cass, A.C.; Alexandrova, A.N.; Anderson, S.L. Ethylene Dehydrogenation on $Pt_{4,7,8}$ Clusters on $Al_2O_3$: Strong Cluster Size Dependence Linked to Preferred Catalyst Morphologies. *ACS Catal.* **2017**, *7*, 3322–3335. [CrossRef]
2. An, W.; Men, Y.; Wang, J.G. Comparative study on hydrogenation of propanal on Ni(111) and Cu(111) from density functional theory. *Appl. Surf. Sci.* **2017**, *394*, 333–339. [CrossRef]
3. Liu, Y.L.; Liu, J.; Feng, G.; Yin, S.; Cen, W.L.; Liu, Y.J. Interface effects for the hydrogenation of $CO_2$ on $Pt_4/\gamma$-$Al_2O_3$. *Appl. Surf. Sci.* **2016**, *386*, 196–201. [CrossRef]
4. Gonda, M.; Ohshima, M.A.; Kurokawa, H.; Miura, H. Toluene hydrogenation over Pd and Pt catalysts as a model hydrogen storage process using low grade hydrogen containing catalyst inhibitors. *Int. J. Hydrogen Energy* **2014**, *39*, 16339–16346. [CrossRef]
5. Shen, W.; Wu, B.; Liao, F.; Jiang, B.; Shao, M. Optimizing the hydrogen evolution reaction by shrinking Pt amount in Pt-Ag/SiNW nanocomposites. *Int. J. Hydrogen Energy* **2017**, *42*, 15024–15030. [CrossRef]
6. Verdinelli, V.; Germán, E.; Jasen, P.; González, E.; Marchetti, J.M. The influence of pre-adsorbed Pt on hydrogen adsorption on B2 FeTi(111). *Int. J. Hydrogen Energy* **2014**, *39*, 8621–8630. [CrossRef]
7. Esan, D.A.; Ren, Y.; Feng, X.; Trenary, M. Adsorption and Hydrogenation of Acrolein on Ru(001). *J. Phys. Chem. C* **2017**, *121*, 4384–4392. [CrossRef]
8. Julkapli, N.M.; Bagheri, S. Graphene supported heterogeneous catalysts: An overview. *Int. J. Hydrogen Energy* **2015**, *40*, 948–979. [CrossRef]
9. Jung, H.; Park, K.T.; Gueye, M.N.; So, S.H.; Park, C.R. Bio-inspired graphene foam decorated with Pt nanoparticles for hydrogen storage at room temperature. *Int. J. Hydrogen Energy* **2016**, *41*, 5019–5027. [CrossRef]
10. Xie, W.; Zhang, Z.; Yang, C.; Wang, M.; Ma, X. Hydrogen generation from water molecule with $Pt_7$ clusters. *Int. J. Hydrogen Energy* **2017**, *42*, 4032–4039. [CrossRef]
11. Avanesian, T.; Gusmão, G.S.; Christopher, P. Mechanism of $CO_2$ reduction by $H_2$ on Ru(0001) and general selectivity descriptors for late-transition metal catalysts. *J. Catal.* **2016**, *343*, 86–96. [CrossRef]
12. Clay, J.P.; Greeley, J.P.; Ribeiro, F.H.; Nicholas Delgass, W.; Schneider, W.F. DFT comparison of intrinsic WGS kinetics over Pd and Pt. *J. Catal.* **2014**, *320*, 106–117. [CrossRef]
13. Liu, D.; Li, G.F.; Yang, F.F.; Wang, H.; Han, J.Y.; Zhu, X.L.; Ge, Q.F. Competition and Cooperation of Hydrogenation and Deoxygenation Reactions during Hydrodeoxygenation of Phenol on Pt(111). *J. Phys. Chem. C* **2017**, *121*, 12249–12260. [CrossRef]
14. Stamatakis, M.; Chen, Y.; Vlachos, D.G. First-Principles-Based Kinetic Monte Carlo Simulation of the Structure Sensitivity of the Water–Gas Shift Reaction on Platinum Surfaces. *J. Phys. Chem. C* **2011**, *115*, 24750–24762. [CrossRef]

15. Taylor, M.J.; Jiang, L.; Reichert, J.; Papageorgiou, A.C.; Beaumont, S.K.; Wilson, K.; Lee, A.F.; Barth, J.V.; Kyriakou, G. Catalytic Hydrogenation and Hydrodeoxygenation of Furfural over Pt(111): A Model System for the Rational Design and Operation of Practical Biomass Conversion Catalysts. *J. Phys. Chem. C* **2017**, *121*, 8490–8497. [CrossRef] [PubMed]
16. Bray, J.M.; Skavdahl, I.J.; McEwen, J.S.; Schneider, W.F. First-principles reaction site model for coverage-sensitive surface reactions: Pt(111)–O temperature programmed desorption. *Surf. Sci.* **2014**, *622*, L1–L6. [CrossRef]
17. Gudmundsdottir, S.; Skulason, E.; Weststrate, K.J.; Juurlink, L.; Jonsson, H. Hydrogen adsorption and desorption at the Pt(110)-(1×2) surface: Experimental and theoretical study. *Phys. Chem. Chem. Phys.* **2013**, *15*, 6323–6332. [CrossRef] [PubMed]
18. Hanh, T.T.T.; Takimoto, Y.; Sugino, O. First-principles thermodynamic description of hydrogen electroadsorption on the Pt(111) surface. *Surf. Sci.* **2014**, *625*, 104–111. [CrossRef]
19. Shi, Q.; Sun, R. Adsorption manners of hydrogen on Pt(100), (110) and (111) surfaces at high coverage. *Comput. Theor. Chem.* **2017**, *1106*, 43–49. [CrossRef]
20. Karlberg, G.S.; Jaramillo, T.F.; Skulason, E.; Rossmeisl, J.; Bligaard, T.; Norskov, J.K. Cyclic voltammograms for H on Pt(111) and Pt(100) from first principles. *Phys. Rev. Lett.* **2007**, *99*, 126101. [CrossRef] [PubMed]
21. Xu, L.S.; Ma, Y.S.; Zhang, Y.L.; Teng, B.T.; Jiang, Z.Q.; Huang, W.X. Revisiting H/Pt(111) by a combined experimental study of the H-D exchange reaction and first-principles calculations. *Sci. China Chem.* **2011**, *54*, 745–755. [CrossRef]
22. Lu, K.E.; Rye, R.R. Flash desorption and equilibration of $H_2$ and $D_2$ on single crystal surfaces of platinum. *Surf. Sci.* **1974**, *45*, 677–695. [CrossRef]
23. Christmann, K.; Ertl, G. Interaction of hydrogen with Pt(111): The role of atomic steps. *Surf. Sci.* **1976**, *60*, 365–384. [CrossRef]
24. Baró, A.M.; Ibach, H.; Bruchmann, H.D. Vibrational modes of hydrogen adsorbed on Pt(111): Adsorption site and excitation mechanism. *Surf. Sci.* **1979**, *88*, 384–398. [CrossRef]
25. Koeleman, B.J.; de Zwart, S.T.; Boers, A.L.; Poelsema, B.; Verheij, L.K. Information on adsorbate positions from low-energy recoil scattering: Adsorption of hydrogen on Pt. *Phys. Rev. Lett.* **1986**, *56*, 1152–1155. [CrossRef] [PubMed]
26. Olsen, R.A.; Kroes, G.J.; Baerends, E.J. Atomic and molecular hydrogen interacting with Pt(111). *J. Chem. Phys.* **1999**, *111*, 11155–11163. [CrossRef]
27. Watson, G.W.; Wells, R.P.K.; Willock, D.J.; Hutchings, G.J. A Comparison of the Adsorption and Diffusion of Hydrogen on the {111} Surfaces of Ni, Pd, and Pt from Density Functional Theory Calculations. *J. Phys. Chem. B* **2001**, *105*, 4889–4894. [CrossRef]
28. Papoian, G.; Nørskov, J.K.; Hoffmann, R. A Comparative Theoretical Study of the Hydrogen, Methyl, and Ethyl Chemisorption on the Pt(111) Surface. *J. Am. Chem. Soc.* **2000**, *122*, 4129–4144. [CrossRef]
29. Mei, D.; Hansen, E.W.; Neurock, M. Ethylene Hydrogenation over Bimetallic Pd/Au(111) Surfaces: Application of Quantum Chemical Results and Dynamic Monte Carlo Simulation. *J. Phys. Chem. B* **2003**, *107*, 798–810. [CrossRef]
30. Mei, D.; Du, J.; Neurock, M. First-Principles-Based Kinetic Monte Carlo Simulation of Nitric Oxide Reduction over Platinum Nanoparticles under Lean-Burn Conditions. *Ind. Eng. Chem. Res.* **2010**, *49*, 10364–10373. [CrossRef]
31. Van Bavel, A.P.; Hopstaken, M.J.P.; Curulla, D.; Niemantsverdriet, J.W.; Lukkien, J.J.; Hilbers, P.A.J. Quantification of lateral repulsion between coadsorbed CO and N on Rh(100) using temperature-programmed desorption, low-energy electron diffraction, and Monte Carlo simulations. *J. Chem. Phys.* **2003**, *119*, 524–532. [CrossRef]
32. Teng, B.T.; Huang, W.X.; Wu, F.M.; Lan, Y.Z.; Cao, D.B. A density functional theory study of the $CH_2I_2$ reaction on Ag(111): Thermodynamics, kinetics, and electronic structures. *J. Chem. Phys.* **2010**, *132*, 024715. [CrossRef] [PubMed]
33. Zhao, Y.; Teng, B.T.; Wen, X.D.; Zhao, Y.; Chen, Q.P.; Zhao, L.H.; Luo, M.F. Superoxide and Peroxide Species on $CeO_2$(111), and Their Oxidation Roles. *J. Phys. Chem. C* **2012**, *116*, 15986–15991. [CrossRef]
34. Teng, B.T.; Lang, J.J.; Wen, X.D.; Zhang, C.; Fan, M.H.; Harris, H.G. $O_2$ Adsorption and Oxidative Activity on Gold-Based Catalysts with and without a Ceria Support. *J. Phys. Chem. C* **2013**, *117*, 18986–18993. [CrossRef]

35. Boekfa, B.; Treesukol, P.; Injongkol, Y.; Maihom, T.; Maitarad, P.; Limtrakul, J. The Activation of Methane on Ru, Rh, and Pd Decorated Carbon Nanotube and Boron Nitride Nanotube: A DFT Study. *Catalysts* **2018**, *8*, 190. [CrossRef]
36. Zhou, J.; Huang, L.; Yan, W.; Li, J.; Liu, C.; Lu, X. Theoretical Study of the Mechanism for $CO_2$ Hydrogenation to Methanol Catalyzed by *trans*-$RuH_2(CO)$(dpa). *Catalysts* **2018**, *8*, 244. [CrossRef]
37. Chen, S.; Luo, J.; Bu, S. Morphology transition of Ag ultrathin films on Pt(111): Kinetic Monte Carlo simulation. *Appl. Surf. Sci.* **2014**, *301*, 289–292. [CrossRef]
38. Prats, H.; Álvarez, L.; Illas, F.; Sayós, R. Kinetic Monte Carlo simulations of the water gas shift reaction on Cu(111) from density functional theory based calculations. *J. Catal.* **2016**, *333*, 217–226. [CrossRef]
39. Exner, K.S.; Heß, F.; Over, H.; Seitsonen, A.P. Combined experiment and theory approach in surface chemistry: Stairway to heaven? *Surf. Sci.* **2015**, *640*, 165–180. [CrossRef]
40. Hong, Q.; Liu, Z. Mechanism of $CO_2$ hydrogenation over Cu/$ZrO_2$(212) interface from first-principles kinetics Monte Carlo simulations. *Surf. Sci.* **2010**, *604*, 1869–1876. [CrossRef]
41. Farkas, A.; Hess, F.; Over, H. Experiment-Based Kinetic Monte Carlo Simulations: CO Oxidation over $RuO_2$(110). *J. Phys. Chem. C* **2012**, *116*, 581–591. [CrossRef]
42. Hermse, C.G.M.; Frechard, F.; van Bavel, A.P.; Lukkien, J.J.; Niemantsverdriet, J.W.; van Santen, R.A.; Jansen, A.P.J. Combining density-functional calculations with kinetic models: NO/Rh(111). *J. Chem. Phys.* **2003**, *118*, 7081–7089. [CrossRef]
43. Van Bavel, A.P.; Hermse, C.G.M.; Hopstaken, M.J.P.; Jansen, A.P.J.; Lukkien, J.J.; Hilbers, P.A.J.; Niemantsverdriet, J.W. Quantifying lateral adsorbate interactions by kinetic Monte-Carlo simulations and density-functional theory: NO dissociation on Rh(100). *Phys. Chem. Chem. Phys.* **2004**, *6*, 1830. [CrossRef]
44. Källén, G.; Wahnström, G. Quantum treatment of H adsorbed on a Pt(111) surface. *Phys. Rev. B* **2001**, *65*, 033406. [CrossRef]
45. Muscat, J.P. Role of multi-adatom interactions in the formation of ordered structures on metal surfaces: Application to H/Fe(110). *Surf. Sci.* **1984**, *139*, 491–504. [CrossRef]
46. Kresse, G.; Hafner, J. Ab initio molecular-dynamics simulation of the liquid-metal amorphous semiconductor transition in germanium. *Phys. Rev. B Condens. Matter* **1994**, *49*, 14251. [CrossRef] [PubMed]
47. Kresse, G.; Furthmüller, J. Efficiency of ab-initio total energy calculations for metals and semiconductors using a plane-wave basis set. *Comp. Mater. Sci.* **1996**, *6*, 15–50. [CrossRef]
48. Perdew, J.P.; Burke, K.; Ernzerhof, M. Generalized Gradient Approximation Made Simple. *Phys. Rev. Lett.* **1996**, *77*, 3865–3868. [CrossRef] [PubMed]
49. Monkhorst, H.J. Special points for Brillouin-zone integrations. *Phys. Rev. B Condens. Matter* **1977**, *16*, 1748–1749. [CrossRef]
50. Kresse, G.; Joubert, D. From ultrasoft pseudopotentials to the projector augmented-wave method. *Phys. Rev. B* **1999**, *59*, 1758–1775. [CrossRef]
51. Jonsson, H.; Mills, G.; Jacobsen, K.W. Nudged elastic band method for finding minimum energy paths of transition. In *CLassical and Quantum Dynamics in Condensed Phase Simulations*; World Scientific: Singapore, 1997; pp. 385–404.
52. Ramalho, J.P.P.; Gomes, J.R.B.; Illas, F. Accounting for van der Waals interactions between adsorbates and surfaces in density functional theory based calculations: Selected examples. *RSC Adv.* **2013**, *3*, 13085–13100. [CrossRef]
53. Prats, H.; Gamallo, P.; Sayos, R.; Illas, F. Unexpectedly large impact of van der Waals interactions on the description of heterogeneously catalyzed reactions: The water gas shift reaction on Cu(321) as a case example. *Phys. Chem. Chem. Phys.* **2016**, *18*, 2792–2801. [CrossRef] [PubMed]
54. Albao, M.A.; Padama, A.A.B. CO adsorption on W(100) during temperature-programmed desorption: A combined density functional theory and kinetic Monte Carlo study. *Appl. Surf. Sci.* **2017**, *396*, 1282–1288. [CrossRef]
55. WELCOME to the CARLOS Project. Available online: https://carlos.win.tue.nl.

56. Núñez, M.; Vlachos, D.G. Steady state likelihood ratio sensitivity analysis for stiff kinetic Monte Carlo simulations. *J. Chem. Phys.* **2015**, *142*, 044108. [CrossRef] [PubMed]
57. Andersen, M.; Plaisance, C.P.; Reuter, K. Assessment of mean-field microkinetic models for CO methanation on stepped metal surfaces using accelerated kinetic Monte Carlo. *J. Chem. Phys.* **2017**, *147*, 152705. [CrossRef] [PubMed]
58. Hu, J.; Teng, B.; Wu, F.; Fang, Y. Fe nanostructures stabilized by long-range interactions on Cu(111): Kinetic Monte Carlo simulations. *New J. Phys.* **2008**, *10*, 023033. [CrossRef]